

Enhanced Removal of Bemacid Blue Anthraquinone Dye by Magnetic Nanocomposite Bentonite-Fe₃O₄: Equilibrium, Kinetic and Thermodynamic Studies

Imane Lacene Necer, Khalil Oukebdane* and Mohamed Amine Didi

Laboratory of Separation and Purification Technology, Department of Chemistry, Faculty of Sciences, Tlemcen University, Box.119, Algeria.

*Corresponding author (e-mail: oukebdane.khalil@yahoo.fr)

Magnetic nanocomposite materials have attracted increasing interest for their use in various scientific applications, including separation processes. The present study investigated the adsorption of the anthraquinone dye Bemacid Blue (BB-dye) on magnetic bentonite (M-Bt) intercalated with iron oxide (Fe₃O₄). The structural and morphological characteristics of the adsorbent were analysed by SEM, XRD, FTIR, BET, and pH_{PZC} techniques. Batch kinetic and equilibrium experiments were conducted to assess the effect of the system variables, i.e., contact time, initial pH, adsorbent dosage, initial dye concentration and temperature. The results showed that the adsorption of the BB-dye was maximal in an acidic medium at pH ≤ 2.5. The adsorption was analysed using Langmuir, Freundlich and Dubinin-Radushkevich (D-R) isothermal models. Adsorption kinetics and isotherms were found to be in good agreement with pseudo 2nd order kinetics and the Langmuir model. From the calculated thermodynamic parameters, the sorption was a spontaneous and exothermic process. Regeneration tests revealed that the magnetic sorbent could be recycled and reused for up to three successive cycles. These results indicate that the prepared nanocomposite M-Bt could be used for BB-dye removal in wastewater treatment considering its advantages such as cost, simplicity of preparation and environmental friendliness.

Keywords: Sorption; Fe₃O₄; bentonite; bemacid blue dye; magnetic nanocomposite

Received: October 2022; Accepted: January 2023

Water pollution is dangerous for public health and the environment. Human activities, whether industrial, urban or agricultural, are at the root of this pollution [1-3]. For instance, synthetic dyes used in the textile industry are discharged directly into nature without any prior treatment, causing serious damage [4]. To overcome this, many studies have been carried out on water depollution during the last few years [2-6].

Textile dyes are classified as refractory and non-biodegradable organic compounds. The treatment of dye-laden effluent is necessary considering its negative impact on human health and aquatic ecosystems, due to its polluting nature and toxicity [4, 6, 7].

To decrease its impact on the environment, a wide range of methods have been developed for the removal of synthetic dyes from waters and wastewaters, such as chemical precipitation, ion exchange, reverse osmosis, electrochemical treatment and membrane technologies. The application of these processes is often limited due to technical or economic constraints [7, 8]. Currently, solid-liquid phase adsorption is one of the most widely-used treatment separation technologies due to its practical operation, recyclability, economy and other advantages [8, 9]. This technique has also been shown in the literature to be very effective in removing dyes from effluent [10, 11]. Researchers

have confirmed the presence of a wide variety of natural materials [12] that have the capacity to fix quantities of organic pollutants present in water, such as activated carbon [13], biosorbents [14], paper mill sludge [15], zeolitic silica [16] etc.

One such material is bentonite, a type of aluminium phyllosilicate clay found naturally that consists mainly of montmorillonite or smectite [17]. It can be used effectively as an adsorbent for the retention of many pollutants and has been given greater consideration due to its low cost, availability, high specific surface area and environmental friendliness [8, 18]. Nevertheless, these natural clays sometimes offer low adsorption affinity for some pollutants such as dyes due to weak adsorbent-adsorbent interactions [19]. An alternative approach would be to use other efficient and more economical adsorbent materials such as magnetic nanocomposites. The use of magnetic materials for the separation of pollutants in effluent is an innovative technology that is gaining attention [2, 20, 21]. It is a promising method which can be used for rapid removal of pollutants from hazardous waste solutions due to its optimal efficiency, lower cost and simplicity [3, 20]. Magnetic nanocomposites have received increased attention due to the presence of multiple active sites and numerous micro-, meso- and macropores for improved adsorption efficiency. They have certain

qualities, including a high specific surface area and easy regeneration compared to other sorbents, which allow them to be considered as excellent adsorbents for the separation of organic and inorganic pollutants [2, 3, 22]. In recent studies, the modification of bentonite clay with metal oxides to form magnetic nano-composites has been favoured to improve its extraction performance towards pollutants [2, 3]. Thus, iron oxide intercalated adsorbents have shown high efficiency, affinity and very fast adsorption kinetics for the decontamination of inorganic and organic pollutants present in wastewater [3,22].

The preparation of a new material with high surface area, excellent adsorption capacity, environmental friendliness and low production cost for the removal of organic and inorganic pollutants remains a challenge for researchers in this field. The present study focused mainly on the synthesis and characterisation of magnetic bentonite (M-Bt) and its potential use for the removal of Bemacid blue dye (BB-dye) from aqueous media. The synthesis of the magnetic nanocomposite was carried out by co-precipitation and characterized by FTIR, XRD, SEM and BET. A batch approach was adopted for the optimization of relevant sorption parameters, such as adsorption kinetics, pH effect, adsorbent dose and initial dye content. The experimental data was investigated using the pseudo-first-order Lagergren kinetic model, the pseudo-second-order model and the intra-particle diffusion model. The thermodynamic parameters ΔG° , ΔH° and ΔS° were also determined.

MATERIALS AND METHODS

1. Reagents

Hydrochloric acid (HCl) and sodium hydroxide (NaOH) were supplied by Merck. Iron (II) sulphate (FeSO₄.7H₂O) and iron (III) chloride (FeCl₃.6H₂O) were obtained from Sigma-Aldrich; all other chemicals and reagents were of analytical grade and used without

any purification. For the desorption procedure, three acids were used: sulphuric acid H₂SO₄, nitric acid HNO₃ and acetic acid CH₃COOH, all supplied by CARLO ERBA.

Synthetic wastewater was prepared using bi-distilled water and the Bemacid N-TF blue dye (sodium 1-amino-4-([3-[(benzoylamino) methyl]-2,4,6-trimethyl phenyl]amino)-9, 10-dioxo-9,10- dihydroanthracene-2-sulfonate, $\lambda_{\max} = 610$ nm, C₃₉H₄₁O₇SN₄Na, M=732.82 g mol⁻¹) provided by the Soitex – Tlemcen textile company (Algeria). The chemical structure of BB-dye is represented in Figure 1. It is an anthraquinone dye, widely used in the textile industry, which is non-degradable and adsorbs poorly to biological solids and therefore remains in the effluent discharge. Different concentrations of BB-dye used in this experiment were prepared by diluting the stock solution with distilled water. The initial pH values of the solutions studied were adjusted using dilute HCl or NaOH.

The clay used in this study was an Algerian montmorillonite, a type of bentonite from Roussel in Maghnia, N.W. Algeria. It was supplied by ENOF Chemical Ltd, 'Non-ferrous' Research Company, and is used in the foundry, ceramics, oil and hydraulic drilling industries.

2. Apparatus

All experiments were performed at room temperature (20 ± 1 °C). For the batch sorption experiments, a multi-station vibrating bench (Haier model) was employed, with a magnetic stirrer (RCT Basic IKAMAG Stirrer with temperature controller ETS-D5). The pH was measured with a WTW 3310 Set-2 digital pH meter. Weighing was performed with an electronic analytical balance (OHAUS). Determination of the dye concentration in the aqueous phase was carried out using a Specord 210 Plus UV-Vis analytical spectrophotometer.

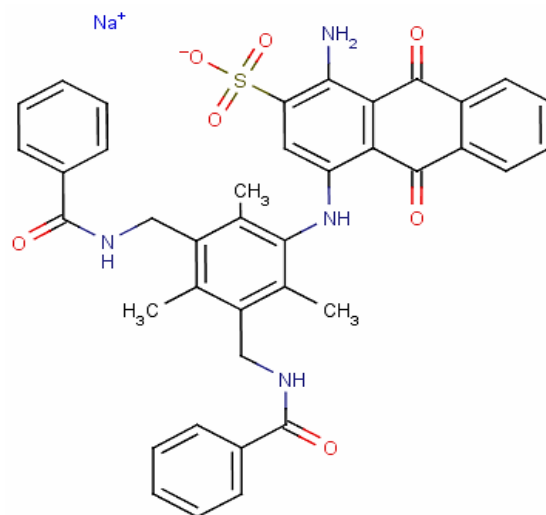


Figure 1. Chemical structure of anionic BB-dye

3. Preparation of Na-Bentonite Clay

The raw sample, obtained from nature, contains impurities that must be removed. After mechanical treatment, the raw sample was reduced to grains of 0.2 mm or less in diameter. The natural clay was washed several times with distilled and deionised water and completely dispersed in water. After 7 h at rest, the dispersion was centrifuged for 1 h at 2000 rpm. The clay particles were then dispersed in water and heated to 70 °C in the presence of a solution composed of the sodium salts of bicarbonate (1 M), citrate (0.3 M) and chloride (2 M) [23]. Then, the bentonite was placed in a NaCl salt solution (1 M) and kept stirring for 12 h (this operation was repeated three times). The purpose of this operation was to remove inorganic and organic compounds. Carbonates and chlorides were removed by treatment with HCl (0.5 M) after several washes. Organic matter was completely removed by treatment with H₂O₂ (30% v/v) at 80 °C for two hours. The clay was then washed several times with distilled water to remove excess salt. To ensure complete conversion to the sodium form, the sample was washed several times with a 0.1 M NaOH solution. After filtration, successive washes with distilled and demineralised water and drying at 100 °C, the clay obtained was labelled Na-Bt and stored in a desiccator.

4. Preparation of Magnetic Bentonite

The co-precipitation method defined by Massart et al [24] using a solution of ferric (3.95 g FeSO₄) and ferrous (7.85 g FeCl₃) salts was used to render the bentonite material magnetic by intercalation of iron oxide particles on its surface [25]. The two solutions (200 mL) were mixed with vigorous stirring and heated to 80 °C under an inert atmosphere. To precipitate the regular sized iron oxides, the pH of the mixture was adjusted to about 9-10 by adding 20 mL NaOH (25%) dropwise until the solution turned black.

Simultaneously, 3 g of bentonite were dispersed in this reaction mixture which was mechanically stirred for 60 min at 70 °C in order to intercalate the iron oxide into the bentonite.

The resulting suspension was then decanted at room temperature and filtered. The final M-Bt residue was washed several times with distilled water to remove the unattached iron oxide ingredients and dried in an oven at 100 °C for 24 h. The magnetic adsorbent was tested using a magnet (0.3 T) to which the impregnated clay particles were attracted.

5. Characterization

All samples in this study were in fine powder form. The crystal structures of the samples were determined by X-ray powder diffraction (XRD) (Rigaku MiniFlex 600 model) for the angle range of 2-80° 2θ (CuKα

radiation, λ = 0.154 nm), operated at a voltage of 40 kV and a current of 15 mA. The magnetized clay samples were investigated using a HITACHI scanning electron microscope (TM-1000) coupled with an Energy Dispersive Spectroscopy (EDS) to determine the topography and grain geometry of the sample. Infrared spectra were obtained between 4000 and 400 cm⁻¹ using a Fourier Transform infrared spectroscopy (FTIR) instrument (Perkin Elmer) using the KBr pellet method. The specific surface areas (SSA) of the samples were determined using a 3Flex Version 5.00 Surface Area Analyzer. Prior to the measurements, the samples were degassed at 150 °C for 8 h, and then the nitrogen adsorption and desorption were measured at 77 °C. For the determination of total surface area and pore size, the Brunauer-Emmet-Teller (BET) method was applied.

The point of zero charge (pH_{pzc}) of the synthesised magnetic bentonite was determined by the salt addition method. A series of sodium chloride solutions at a concentration of 0.1 (mol.L⁻¹) were prepared with different pH values ranging from 1 to 12. Then, 0.1 g of M-Bt was added to each salt solution and the resulting suspension was stirred for 24 hours at room temperature. The final pH was measured and the ΔpH of the solutions were plotted against the initial pH values. The pH_{pzc} is equal to the initial pH, based on which the M-Bt nanocomposite does not change the pH of the solution (ΔpH=0).

6. Adsorption Procedure

Bemacid blue dye was chosen as a model organic pollutant to evaluate its adsorption by magnetic bentonite. A precise mass of adsorbent was used for the adsorption of a 5 ml solution of BB-dye at different concentrations ranging from 1 to 100 mg L⁻¹. The effect of adsorbent mass was studied by varying its mass from 0.005 g to 0.100 g. The adsorption kinetics were studied by analysing the samples as a function of time.

The pH factor was studied by adjusting the pH of the solutions in the interval 1-9 with dilute NaOH and HCl solutions. To evaluate the thermodynamic adsorption parameters, tests on the effect of temperature on adsorption were carried out between 10 and 50 °C. At the end of the experiments, the magnetic nanocomposite was collected by an external magnet (0.3 Tesla) and the amount of residual dye was analysed. Each experiment was repeated three times, and the average results were recorded. The relative standard deviation (RSD) was determined between 2 and 5% for each point in all experiments.

The concentration of residual dye in the solution was determined using a UV-Visible spectrophotometer by measuring the absorbance at the maximum wavelength (λ_{max} = 610 nm) of BB-dye. The removal efficiency

(R%) and adsorption capacity (q) of the adsorbent were calculated using Equation 1 and 2 respectively:

$$R\% = \frac{C_0 - C}{C_0} \times 100 \quad (1)$$

$$q(mg/g) = \frac{(C_0 - C_e) \times V}{m} \quad (2)$$

where C₀ (mg L⁻¹) represents the initial concentration of Bemacid blue dye, C (mg L⁻¹) is the concentration of Bemacid blue in solution after adsorption, V (L) is the volume of the aqueous solution, and m (g) is the mass of adsorbent.

The adsorption mechanism and kinetics were correlated by common adsorption isotherms and kinetic models respectively.

RESULTS AND DISCUSSION

The use of bentonite was justified by the fact that it is an inexpensive and environmentally friendly adsorbent material. However, M-Bt was prepared by intercalating iron oxide on the surface of the bentonite. After preparation, a test with a 0.3 T magnet proved that the whole material was magnetic and completely attracted to the magnet.

1. Characterisation

The raw clay was characterised by different methods, namely: Fourier transform infrared spectroscopy (FTIR), X-ray powder diffraction (XRD) analysis, scanning electron microscopy (SEM), BET surface and porosity measurements and X-ray fluorescence spectrometry (XRF).

The chemical composition of the bentonite as determined by XRF is reported in Table 1. Silica and alumina were its main constituents, with minor traces of sodium, potassium, iron, magnesium and calcium oxides as impurities.

From these results, it is clear that the natural bentonite of Maghnia was characterized by a calcium oxide (CaO) content lower than that of sodium oxide (Na₂O), thus the Na₂O/CaO ratio is higher than 1, indicating the presence of sodium bentonite in the samples.

Also, the raw clay was composed mainly of silicate and is rich in alumina, with a SiO₂/Al₂O₃ ratio of 3.78 that is consistent with montmorillonites, which have a ratio of between 2 and 5.5 [26, 27]. Some authors present this ratio as the degree of purity of a bentonite in terms of its montmorillonite content [28, 29]. The composition of the other oxides (MgO, K₂O, CaO and Na₂O) reached 9.18 %, which shows that the clay sample was not pure and contained exchangeable cations like Mg²⁺, K⁺, Ca⁺ or Na⁺.

The FTIR spectra of Na-Bt and the M-Bt nanocomposite are shown in Figure 2. The FTIR spectra of the two forms of bentonite were similar. The absorption band at 3642 cm⁻¹ was attributed to the stretching vibration of montmorillonite structural -OH groups and the bands at 3428 cm⁻¹ and 1647 cm⁻¹ corresponded to the stretching vibration and the bending vibration of H₂O, respectively. A characteristic absorption band of the Si-O stretching vibration was observed at 1045 cm⁻¹ [30]. The band at 920 cm⁻¹ was identified as corresponding to the Al-Al-OH bending vibration [31]. Those at 521 cm⁻¹ and 461 cm⁻¹ were due to the Al-O-Si and Si-O-Si bending vibrations, respectively [30].

Table 1. Chemical composition of raw bentonite (ENOF-Tlemcen)

Oxide	SiO ₂	Al ₂ O ₃	MgO	Fe ₂ O ₃	Na ₂ O	CaO	K ₂ O	TiO ₂	other species
Composition (%)	65.20	17.25	5.33	2.22	1.50	1.23	1.15	1.06	≤ 1

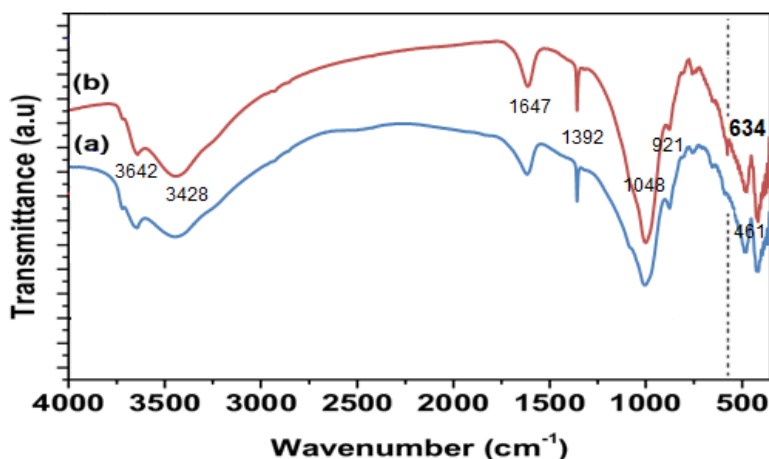


Figure 2. FTIR spectra of (a) Na-Bt and (b) M-Bt.

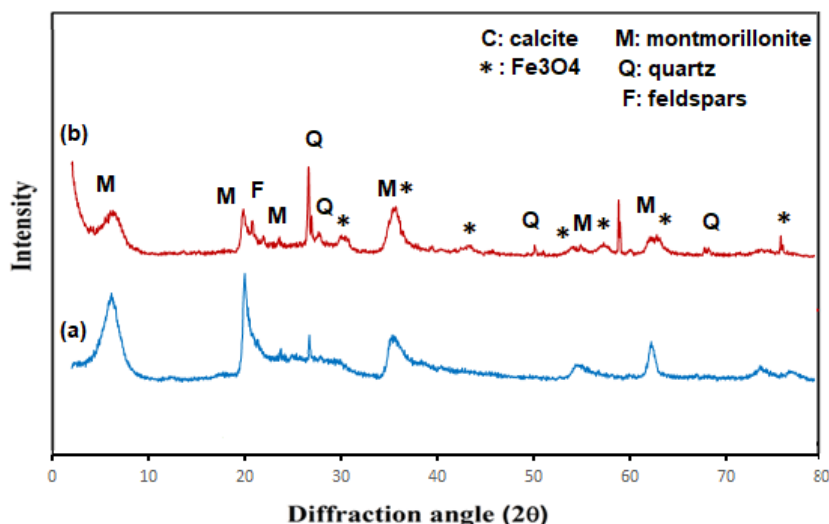


Figure 3. XRD patterns of (a) Na-Bt and (b) M-Bt

The peak at 634 cm⁻¹ in the infrared spectrum of the composite was assigned to the characteristic peak of the Fe-O group indicating that the magnetic Fe₃O₄ particles had been successfully loaded onto the bentonite surface to produce magnetic bentonite [32-34]. In addition, it also confirms that the new material maintained the basic structure of bentonite.

Figure 3 shows the XRD patterns of the two forms of bentonite. As can be seen in Figure 3(a), the diffraction peaks corresponding to the bentonite structure were also present in the XRD pattern of the magnetic composite, indicating that the montmorillonite structure was not destroyed after the chemical coprecipitation of iron oxide [27, 31, 33]. Some additional peaks were also present, which correspond to quartz (Q), feldspar and CaCO₃ minerals. The XRD pattern of the magnetic bentonite in Figure 3(b) shows the main diffraction peaks at 2θ = 30.09°, 36.45°, 44.08°, 54.76°, 58.29°, 64.26°, and 74.09° which refer to the (111), (220), (311), (400), (422), (511), and (440) crystal faces respectively. These peaks are related to the presence of magnetite in agreement with the standard peaks for spinel, Fe₃O₄ (JCPDS No.3-863) [32-35] which indicates the success of the Fe(II), Fe(III) intercalation method

in montmorillonite clay and confirms the formation of a magnetic clay. Some weak diffraction peaks were also observed, which can be attributed to goethite (α-FeOOH) and hematite (α-Fe₂O₃). It must be noted that the width of some lines may have resulted from the small size of the particles obtained or poorly crystallised iron oxides.

Similarly, the SEM results for both forms of bentonite are shown in Figure 4. It is clear from Figure 4(a) that the surface has an irregular porous structure with large spaces, making it suitable for use as an adsorbent. On the other hand, the SEM results of the M-Bt nanocomposite showed a fluffier surface with small irregular pores which proved the presence of a higher proportion of small diameter grains compared to the Na-Bt sample, and confirmed the successful impregnation of iron oxide onto the bentonite surface. The distribution and dispersion of the iron oxide nanoparticles on the bentonite surface is generally due to their magnetic nature which has a strong tendency to self-agglomerate en masse [36]. This shows that the granules increase the surface roughness and porosity of the adsorbent, thus significantly improving the surface characteristics and adsorption efficiency of the bentonite clay.

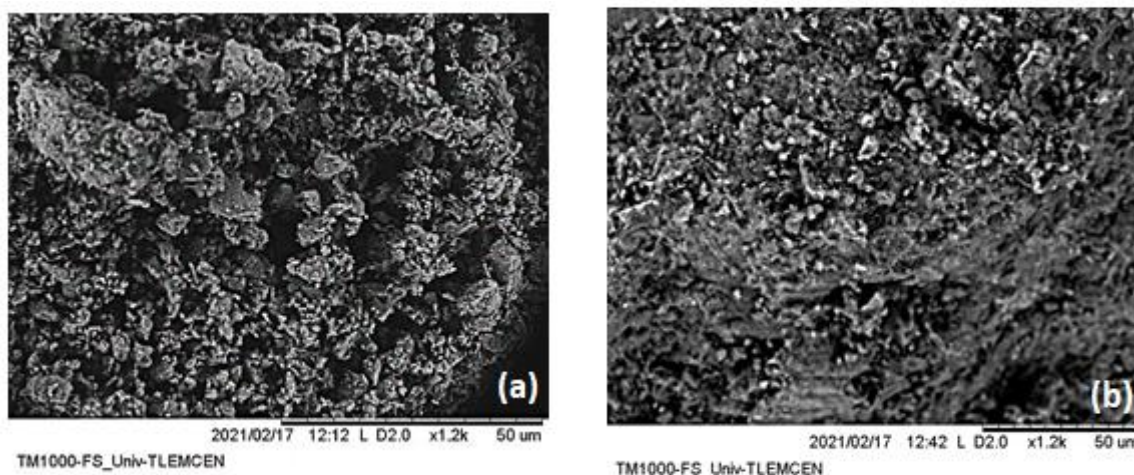
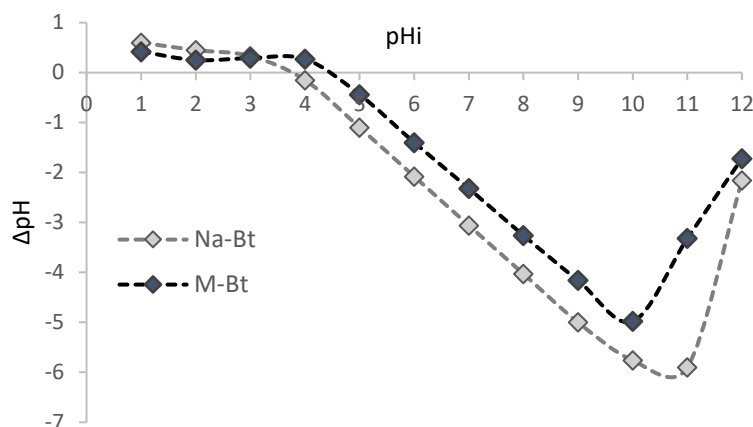


Figure 4. SEM images of bentonite clays (a) Na-Bt (b) M-Bt

Table 2. BET surface area, total pore volume and average pore size of Na-Bt and M-Bt

Sample	Na-Bt	M-Bt
BET surface area (m ² g ⁻¹)	88.88	113.34
Microporous surface area (m ² g ⁻¹)	29.00	12.13
Total pore volume (cm ³ g ⁻¹)	0.14	0.23
Micropore volume (cm ³ g ⁻¹)	0.013	0.005
Average pore size (nm)	8.63	10.37
Average mesopore size (nm)	5.79	7.54

**Figure 5.** Point of zero charge (pH_{PZC}) of sodic and magnetic bentonite

Adsorption occurs mainly on the surface of solid adsorbents. Therefore, the surface structure is a crucial factor that determines adsorption performance. Table 2 shows a significant increase in the specific surface area (113.34 m²/g) of M-Bt compared to Na-Bt; however, the surface area of the micropores was reduced. The average total pore size and the average mesopore size of M-Bt were both higher compared to Na-Bt. This is probably due to the Fe₃O₄ particles that penetrated the bentonite layers and pore channels covering the surface. This provides further evidence that Fe₃O₄ particles had successfully grafted onto the bentonite surface.

The point of zero charge analysis (PZC) is a fundamental property that provides information on the electrical neutrality of the adsorbent surface at a particular pH and constitutes a reference for further studies on adsorption performance. The PZC values of the adsorbents were determined by the salt addition method previously reported in the literature [37].

The graph of ΔpH (pH_{initial}-pH_{final}) versus pHi_{initial} was plotted as shown in Figure 5. The pH_{PZC} values were determined for sodic and magnetic bentonite from the intersection point of the curves with the X-axis, which corresponded to pH 3.9 and pH 4.5, respectively. This indicates that the presence of magnetic nanoparticles on the surface of the bentonite changed its charging properties rather than its surface morphology. The PZC value also reveals that cation adsorption was favoured at pH > pH_{PZC}, while anion adsorption was

favoured at pH < pH_{PZC}.

2. Adsorption Study

2.1. Effect of pH

The pH of a solution is generally recognized as an important parameter that influences the adsorption process. To understand this phenomenon, the zero-charge point (pH_{PZC}) values of sodic and magnetic bentonite were determined by the salt addition method [38]. Figure 6 shows the effect of pH on the adsorption of BB-dye on sodic and magnetic bentonite.

In order to study the effect of pH, three different phases were tested: acidic, neutral and alkaline. Thus, experiments were conducted with pH values ranging from 1 to 9.

This decrease in adsorption efficiency is in agreement with other studies [22, 39-42], since BB-dye is an anionic dye in aqueous solution with a negative charge due to the presence of sulphonate groups (SO⁻³), which are preferentially adsorbed. The highest BB-dye removal was in an acidic medium pH < pH_{PZC} and this was mainly due to the strong attraction between the positively charged active sites and negatively charged BB-dye groups. In a basic medium pH > pH_{PZC}, the removal of BB-dye was lower, and this may be due to the competition of OH⁻ ions with (BB-dye)⁻ ions for the same active sites in the material.

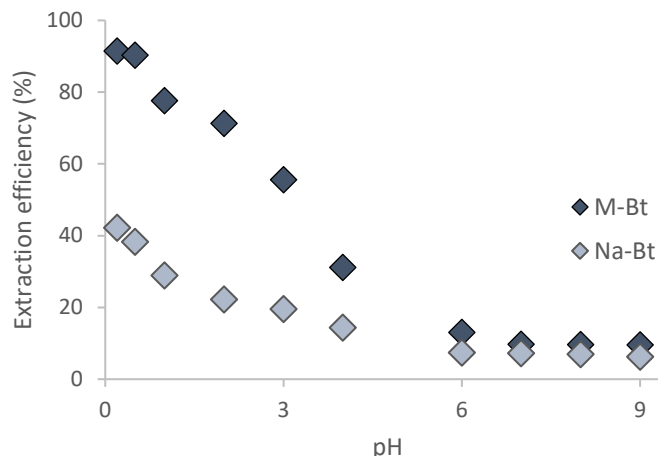


Figure 6. Effect of pH on the adsorption of BB-dye by Na-Bt and M-Bt ($[C_0]_{\text{BB-dye}} = 50 \text{ mg. L}^{-1}$, $m = 0.01 \text{ g}$, $\Phi = 300 \text{ rpm}$, $T = 20 \text{ }^\circ\text{C}$)

Changing the surface of aluminosilicate minerals with magnetic nanoparticles has led to a new class of nanocomposite materials, which could also be used for environmental applications as adsorbents of organic and inorganic compounds and metal ions. Consequently, the results of the BB-dye adsorption were more satisfactory with M-Bt than with Na-Bt, so this study focused on magnetic bentonite.

2.2. Effect of Adsorbent Mass

The effect of the sorbent mass on dye removal was investigated to determine the optimum amount of magnetic bentonite required for BB-dye sorption and the results are presented in Figure 7. The mass of magnetic bentonite used was in the range of 0.005-0.100 g, while the initial dye concentration was 50 mg L⁻¹ and the time of sorption was 60 min.

As shown in Figure 7, the increase in BB-dye

sorption yields with sorbent mass can be attributed to the increase in sorbent surface area and the availability of a greater number of sorption sites.

Also, the amount of dye adsorbed per gram of adsorbent decreased with the increasing mass of M-Bt. By increasing the amount of sorbent, the probability of collision between solid particles increases and leads to an aggregation of the particles, resulting in a decrease of the total surface area and an increase of the diffusion path length [43]. Another possible interpretation is the reduced unsaturation of the adsorption sites and thus the decrease in the number of these sites per unit mass [44], as well as the adsorption driving force (concentration of dye molecules/ concentration of adsorption sites) [45]. As the dose of M-Bt increased, aggregation also increased, leading to a fewer active sites and thus a decrease in adsorption. For further experiments, 0.01 g of M-Bt was used.

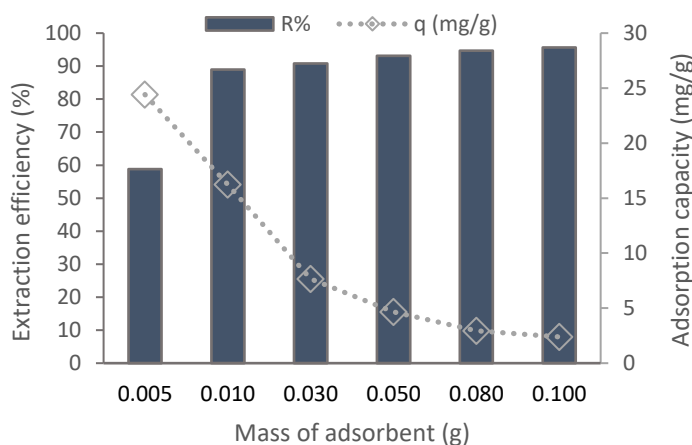


Figure 7. Effect of sorbent quantity on BB-dye adsorption ($[C_0]_{\text{BB-dye}} = 50 \text{ mg.L}^{-1}$, $\Phi = 300 \text{ rpm}$, $V = 5 \text{ mL}$, $T = 20 \text{ }^\circ\text{C}$)

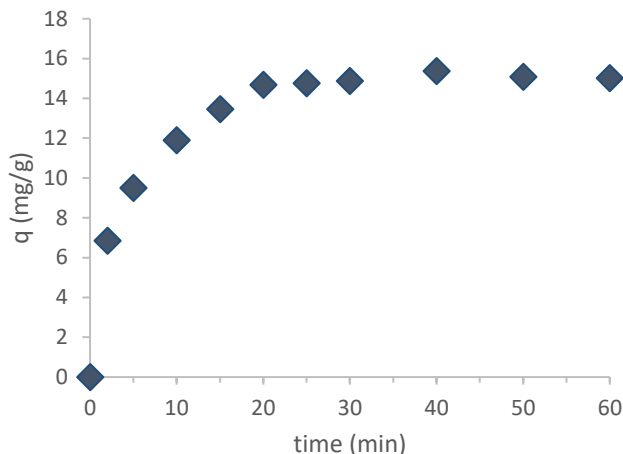


Figure 8. Adsorption kinetics of BB-dye by M-Bt ($[C_0]_{\text{BB-dye}} = 50 \text{ mg. L}^{-1}$, $m = 0.01 \text{ g}$, $\Phi = 300 \text{ rpm}$, $V = 5 \text{ ml}$, $T = 20 \text{ }^\circ\text{C}$)

2.3. Contact Time Effect

The contact time was studied to determine the optimal time for BB-dye removal efficiency. Figure 8 shows the effect of contact time on the adsorption capacity of BB-dye by M-Bt. The adsorption capacity of bentonite increased with contact time, and after about 30 minutes almost all the dye had been extracted by M-Bt. This rapid adsorption of the dye was due to a high affinity between the dye molecules and the active sites on the surface of the bentonite.

2.4. Effect of Concentration

The effect of the initial dye concentration was studied by mixing a volume of BB-dye solution at a solution pH of 2.5, with M-Bt (0.01 g) and stirring the solution at 300 rpm until equilibrium. It was observed from

Figure 9 that the amount of BB-dye adsorbed increased significantly from 0.342 to 17.08 mg g⁻¹ with increasing initial dye concentration.

These results were due to the driving forces provided by the initial concentration to overcome the mass transfer resistance of BB-dye molecules between the liquid and solid phases during adsorption. Consequently, an increased initial concentration of dye enhanced the adsorption process [22, 33].

2.5. Adsorption Kinetics

The adsorption kinetics of the reaction were studied to validate the adsorption mechanism between the adsorbent and the studied solute. Pseudo-first order, pseudo-second order and intra-particle diffusion models were used in the evaluation.

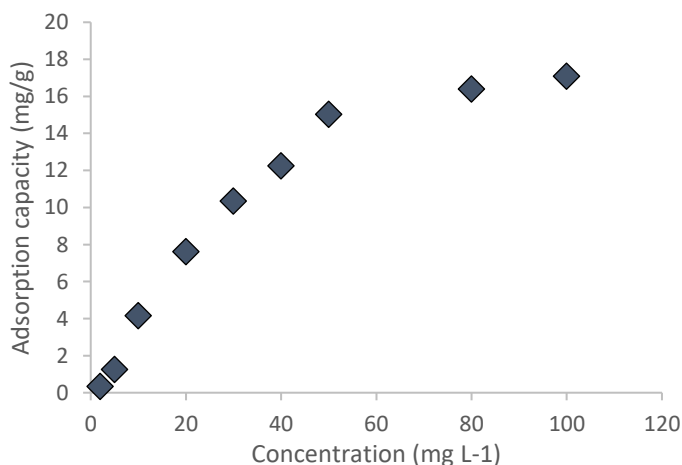


Figure 9. Adsorption capacity as a function of initial BB-dye concentration ($m = 0.01 \text{ g}$, $\Phi = 300 \text{ rpm}$, $\text{time} = 30 \text{ min}$, $T = 20 \text{ }^\circ\text{C}$)

Table 3. Kinetic data for BB-dye adsorption by M-Bt

Model	Pseudo-first order			Pseudo-second order			Intraparticle diffusion		
Parameter	K ₁	q _e	R ²	K ₂	q _e	R ²	k _d	S	R ²
M-Bt	0.175	13.75	0.976	0.027	15.82	0.999	2.548	3.551	0.992

Lagergren's pseudo-first order kinetic model was applied to verify the adsorption of BB-dye from aqueous solution. The linear form of the pseudo-first order equation is described by Lagergren as follows:

$$\ln(q_e - q) = \ln q_e - k_1 t \quad (3)$$

The pseudo-second order model can be expressed by Equation 4:

$$\frac{t}{q} = \frac{1}{q_e^2 k_2} + \frac{t}{q_e} \quad (4)$$

where q_e and q are the amounts of adsorbed dye (mg g⁻¹) at equilibrium and time t , respectively, k_1 is the rate constant (min⁻¹) of the pseudo-first order model and k_2 is the rate constant of the pseudo-second order model (g mg⁻¹ min⁻¹).

For intraparticle diffusion, the adsorption of BB-dye is generally governed by either the liquid phase mass transport rate or the intraparticle mass transport rate [46]. This model was represented by Equation 5:

$$q = K_d \times t^{1/2} + S \quad (5)$$

where K_d is the constant for intra-particle diffusion (mg g⁻¹ min^{1/2}) and S is a constant that explains the boundary layer effect.

The parameter values for the adsorption of BB-dye by M-Bt are presented in Table 3.

The best-fit model was determined based on the calculation of the linear correlation coefficients R^2 . Application of the kinetic models (Table 3) for the removal of BB-dye by M-Bt showed that the data obtained was in better agreement with the pseudo-second order model ($R^2 = 0.999$) compared to the pseudo-first order model ($R^2 = 0.976$). In addition, the adsorption capacity (q_e) obtained with the pseudo-second order model was in agreement with the experimental value calculated from the equilibrium sorption kinetics. For the intraparticle diffusion study, the R^2 value was 0.992. However, the failure of the curve to pass through the origin indicated that intraparticle diffusion was involved in the adsorption process but was not the only rate-limiting mechanism, and that other mechanisms such as complexation or ion exchange also had important roles [22, 33, 46].

2.6. Adsorption Isotherm

Adsorption isotherm modelling is widely used to describe the adsorption process and to elucidate adsorption mechanisms [3, 33, 39, 47]. It allows one to define the interaction properties of the adsorbed molecules with the adsorbent surface. The adsorption mechanism of BB-dye on magnetic bentonite was evaluated using three (Langmuir, Freundlich and Dubinin-Radushkevich (D-R)) isothermal models.

The Langmuir model assumes that the adsorption process occurs in a monolayer form with homogeneous active sites distributed over the entire surface of the adsorbent under study without any interaction between the adsorbed ions [48]. The following linearization of the Langmuir Equation can be written as:

$$\frac{C_e}{Q_e} = \frac{C_e}{Q_m} + \frac{1}{Q_m \cdot k_L} \quad (6)$$

where C_e (mg L⁻¹) is the equilibrium dye concentration, Q_e and Q_m (mg g⁻¹) are the equilibrium and maximum adsorption capacity of the adsorbents, respectively, and k_L is the Langmuir isotherm constant.

By plotting the line $C_e/q_e = f(C_e)$ and using the slope, the values of the monolayer capacity Q_m and the Langmuir parameter K_L are determined. An essential characteristic of the Langmuir isotherm was formulated by a dimensionless constant called the separation factor, R_L [33] given by the following Equation 7:

$$R_L = \frac{1}{1 + K_L C_0} \quad (7)$$

where, C_0 is the initial dye concentration.

The value of R_L indicates the type of isotherm: unfavourable when $R_L > 1$, linear if $R_L = 1$, favourable if $0 < R_L < 1$ or irreversible when $R_L = 0$.

The Freundlich isotherm is applicable to non-ideal adsorption; it assumes that adsorption is a heterogeneous process and that any increase in the adsorption capacity leads to an exponential decrease in the binding energy of the multilayer forming surface of the different adsorbed molecules [48]. The Freundlich isotherm model is expressed by Equation 8:

$$\ln(Q_e) = \ln kf + \frac{1}{n} \ln(C_e) \quad (8)$$

where k_f and n are Freundlich isotherm constants associated with the maximum adsorption of material, and are determined from the intercept and slope of the graph of $\ln(q_e)$ vs $\ln(C_e)$ respectively [48].

The D-R model is an empirical model that can be used to describe the nature of the adsorption, whether it is physical or chemical [13, 33]. The linear equation of the D-R model is expressed by Equation 9:

$$\ln q_e = \ln q_m - B\varepsilon^2 \quad (9)$$

$$\varepsilon = RT \ln \left(1 + \frac{1}{C_e} \right) \quad (10)$$

where B is a constant, q_m (mg g⁻¹) is the adsorption saturation capacity and ε is the Polanyi potential which can be calculated using Equation 10. The parameter β may be used for estimating the average free energy $E=1/\sqrt{(2 \times \beta)}$ to distinguish the type of adsorption process. When E is < 8 KJ mol⁻¹, the adsorption process is physical adsorption, but when E is between 8 and 16 kJ mol⁻¹, the process is chemical adsorption [49]. The modelling parameters were calculated and reported in Table 4.

The correlation coefficient (R^2) determines which model is more appropriate for the adsorption process. The R^2 values obtained with the Langmuir (0.998), Freundlich (0.934) and D-R (0.995) models indicate that the experimental isotherm data was best fit by the Langmuir model, suggesting that the adsorption of BB-dye by M-Bt formed a monolayer of dye on the adsorbent surface. In addition, the calculated R_L value

was between 0.765 and 0.061, indicating that the adsorption process was favourable. As with the D-R model, the magnitude of the E value was evaluated to assess the adsorption mechanism. The value of E (7.9 kJ mol⁻¹) was lower than 8 kJ mol⁻¹ suggesting that the adsorption of BB-dye in the aqueous phase by M-Bt was mainly a physisorption process.

2.7. Thermodynamic Parameters

Temperature is a very important element in the sorption process. Therefore, the thermodynamic data is the best indicator for the practical application of such a process. The quantity of BB-dye adsorbed at a range of temperatures (10-50 °C) was determined in order to calculate the thermodynamic parameters of the adsorption system. The free energy change (ΔG°), enthalpy change (ΔH°) and entropy change (ΔS°) values were calculated using the following equations:

$$K_d = \frac{qe}{Ce} \quad (11)$$

$$\ln(K_d) = \frac{\Delta S^\circ}{R} - \frac{\Delta H^\circ}{RT} \quad (12)$$

$$\Delta G^\circ = \Delta H^\circ - T\Delta S^\circ \quad (13)$$

where K_d is the distribution coefficient for the adsorption, T is the temperature (K) and R is the universal gas constant (J mol⁻¹ K⁻¹). The enthalpy (ΔH°) and entropy (ΔS°) values were calculated from the slope and intercept of the plot of $\ln K_d$ versus $1/T$ (Figure 10).

Table 4. Isothermal constants for BB-dye adsorption on M-Bt

Parameter	Langmuir model			Freundlich model			D-R model		
	k_L	q_m	R^2	k_F	n_F	R^2	$E(\text{kJ.mol}^{-1})$	β	R^2
M-Bt	0.146	18.83	0.998	3.980	2.597	0.934	7.91	$8E^{-09}$	0.995

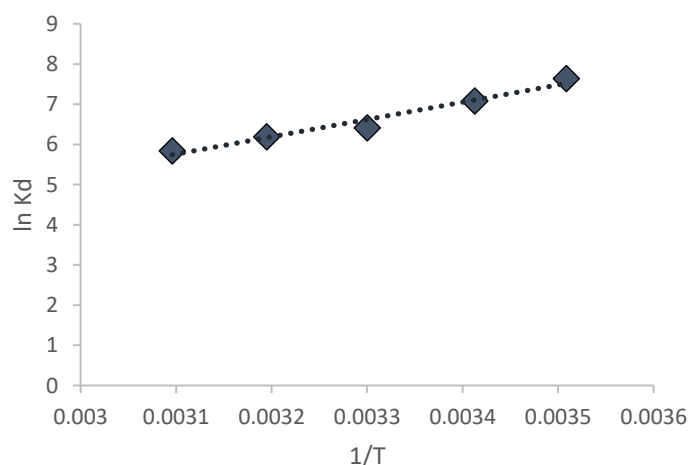


Figure 10. $\ln(K_d)$ versus $1/T$ plot of BB-dye adsorption

Table 5. Thermodynamic parameters for BB-dye adsorption by M-Bt

	T(K)	Ln(K _a)	ΔG° (Kj.mol ⁻¹)	ΔH° (Kj.mol ⁻¹)	ΔS° (j.mol ⁻¹)
	283	7.637	-18.096		
	293	7.078	-17.242		
M-Bt	303	6.410	-16.149	-35.759	-62.924
	313	6.192	-16.113		
	323	5.836	-15.672		

The thermodynamic parameters are reported in Table 5.

The negative values of ΔG° reflect the thermodynamic feasibility and spontaneity of the BB-dye sorption process. The decrease in negative ΔG° values associated with increasing temperatures reveals an increase in the feasibility of sorption at higher temperatures. The value of ΔH° was -35.76 kJ mol⁻¹, which indicates the exothermic nature of the sorption process. On the other hand, the negative value of ΔS° implies a decrease in randomness at the soil-solution interface during the binding of the BB-dye to the active sites of the sorbent [50].

3. Regeneration and Reuse of Sorbent

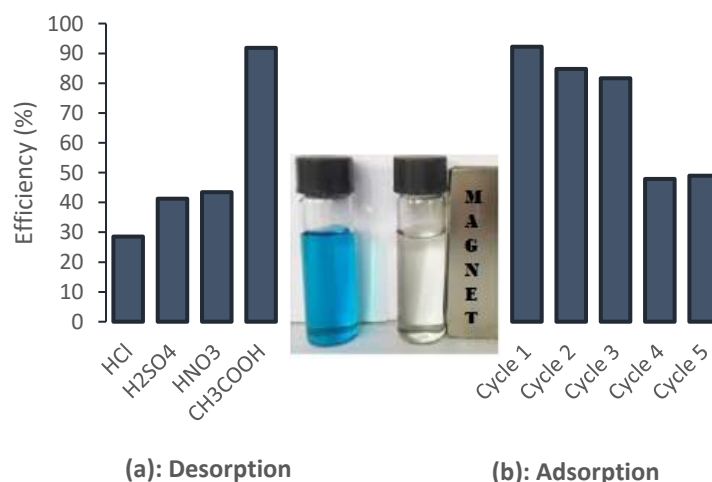
The regeneration and reuse of adsorbents are important parameters in assessing their potential for commercial applications. Magnetic bentonite was first saturated with a known solution of BB-dye. After the adsorption process, the contaminated bentonite samples were treated with four eluents with a concentration of 0.1 mol L⁻¹: hydrochloric acid (HCl), nitric acid (HNO₃), sulphuric acid (H₂SO₄), and acetic acid (CH₃COOH). The above-mentioned desorption solutions were chosen to avoid damaging the adsorbent and/or changing its physical structure. The results obtained are presented in Figure 11.

Figure 11(a) shows that the percentage desorption of CH₃COOH (in one step) was higher than that of other desorbing solutions for the anionic BB-dye, with a maximum elution yield of > 90 %. Next, adsorption experiments were performed with 0.1 g M-Bt in 5 mL of BB-dye solutions for five cycles with the aim of reusing the adsorbent.

As shown in Figure 11(b), the percentage of BB-dye adsorption decreased non-significantly from 92.2 to 81.6% after three cycles. This suggests that M-Bt can be recycled and reused for up to three successive cycles with an adsorption efficiency of > 81 %.

4. Proposed BB-dye/M-Bt Interactions

Different potential interactions for the adsorption of cationic and anionic dyes have been suggested in the literature, such as electrostatic attraction, ion exchange, hydrogen bonding, pore filling and n-π interactions [22, 51, 52]. In general, the adsorption mechanism depends on the physicochemical properties of the adsorbate-adsorbent couple and different factors that affect the adsorption process such as pH, solute concentration, adsorbent dose, temperature, contact time and stirring speed.

**Figure 11.** Regeneration study (adsorption/desorption) of bentonite

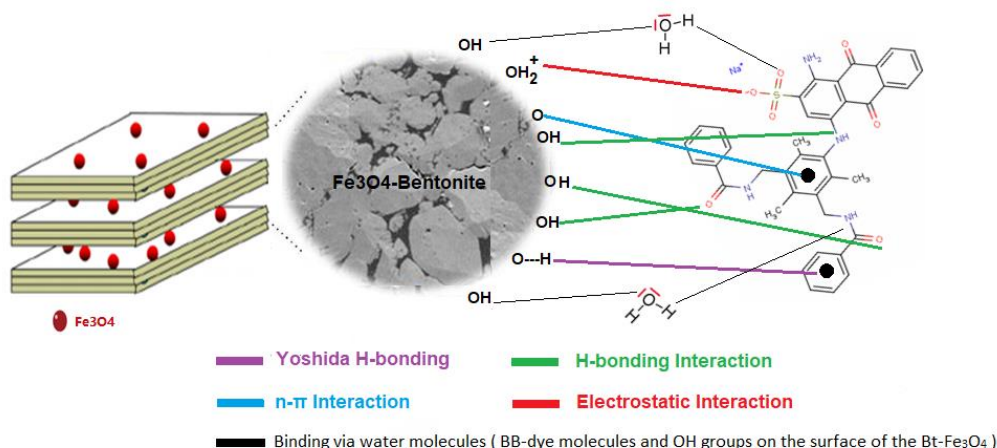


Figure 12. Proposed interactions between M-Bt and BB-dye

The most favourable extraction conditions for the adsorption process occur at $\text{pH} < \text{pH}_{\text{pzc}}$. Under these conditions, the surface of the magnetic nanocomposite M-Bt is predominantly positively charged, which allows weak electrostatic interactions with the active sites present on its surface [33]. This mechanism can occur through (Figure 12):

- Electrostatic interactions between the functional groups (S-OH) present on the surface of the magnetic bentonite and the BB-dye molecules.
- The formation of hydrogen bonds between the amine and hydroxyl groups present in the chemical structure of the BB-dye and OH group oxygens of the iron oxide Fe₃O₄ at the bentonite surface.
- Binding via water molecules, which bind with both dye molecules and the hydroxide groups on the surface of the M-Bt nanocomposite.
- Yoshida H-bond interactions between the -OH groups and the aromatic rings of the BB-dye.
- n- π interactions (also known as n- π electron donor-acceptor interactions).

CONCLUSION

In this study, the adsorption properties of bentonite and the magnetic power of iron oxides were combined to make a magnetic adsorbent. This magnetic nanocomposite showed great potential as an adsorbent for anthraquinone dyes present in water. XRD and SEM results indicated that the nanocomposite particles had good crystallinity with a regular morphology and a homogeneous particle size distribution. FTIR spectroscopy confirmed the structure of the iron oxide nanoparticles intercalated on the bentonite.

BB-dye adsorption was studied by a batch process and it was observed that > 90 % of the dye was removed using 0.01 g of M-Bt. The higher adsorption

of BB-dye at low pH values was attributed to an adsorption mechanism governed mainly by electrostatic interactions between the positively charged bentonite surface and the anionic dye species, as well as by hydrogen and dipole-dipole interactions. However, the considerable increase in adsorption proved that n- π and hydrogen interactions were also involved in the process. The adsorption isotherms and kinetic data fit well with Langmuir and pseudo-second order kinetic models, respectively. The thermodynamic parameters proved that the process was spontaneous and exothermic. From these results, the M-Bt nanocomposite promises to be an effective and economical material for the removal of pollutants in a practical environmental remediation process.

DATA AVAILABILITY

All data generated or analysed during this study are included in this published article.

ACKNOWLEDGMENTS

The authors would like to thank to DGRSDT and ATRST-Algeria for their financial support.

AUTHORS' CONTRIBUTIONS

All authors reviewed and approved the final manuscript and contributed equally.

DECLARATIONS CONFLICT OF INTEREST

The authors confirm that this article content has no conflict of interest.

REFERENCES

- Donkadokula, N. Y., Kola, A. K., Naz, I. and Saroj, D. (2020) A review on advanced physico-chemical and biological textile dye wastewater treatment techniques. *Reviews in Environmental Science and Biotechnology*, **19**, 543–556.

- 155 Imane Lacene Necer, Khalil Oukebdane and Mohamed Amine Didi
- Enhanced Removal of Bemacid Blue Anthraquinone Dye by Magnetic Nanocomposite Bentonite-Fe₃O₄: Equilibrium, Kinetic and Thermodynamic Studies
2. Nithya, R., Thirunavukkarasu, A., Sathya, A. B. and Sivashankar, R. (2021) Magnetic materials and magnetic separation of dyes from aqueous solutions: a review. *Environmental Chemistry Letters*, **19**, 1275–1294.
 3. Panda, S. K., Aggarwal, I., Kumar, H., Prasad, L., Kumar, A., Sharma, A., Vo, D. V. N., Thuan, D. V. and Mishra, V. (2021) Magnetite nanoparticles as sorbents for dye removal: a review. *Environmental Chemistry Letters*, **19**, 2487–2525.
 4. Kishor, R., Purchase, D., Saratale, G. D., Saratale, R. G., Ferreira, L. F. R., Bilal, M., Chandra, R. and Bharagava, R. N. (2021) Ecotoxicological and health concerns of persistent coloring pollutants of textile industry wastewater and treatment approaches for environmental safety. *Journal of environmental chemical engineering*, **9**, 105012.
 5. Samsami, S., Mohamadizani, M., Sarrafzadeh, M. H., Rene, E. R. and Firoozbahr, M. (2020) Recent advances in the treatment of dye-containing wastewater from textile industries: Overview and perspectives. *Process Safety and Environmental Protection*, **143**, 138–163.
 6. Dhruv Patel, D. and Bhatt, S. (2022) Environmental pollution, toxicity profile, and physico-chemical and biotechnological approaches for treatment of textile wastewater. *Journal of Genetic Engineering and Biotechnology*, **38**, 33–86.
 7. Mansoori, S. M., Yamgar, R. S. and Rathod, S. V. (2021) Synthesis of Zinc-Copper-Iron (II, III) Oxide Nanocomposites and their Photocatalytic Efficiency for Crystal Violet Degradation. *Malaysian Journal of Chemistry*, **23**(1), 15–23.
 8. Crini, G. (2006) Non-conventional low-cost adsorbents for dye removal. *Bioresource Technology*, **97**, 1061–1085.
 9. Dąbrowski, A. (2001) Adsorption—from theory to practice. *Adv. Journal of Colloid and Interface Science*, **93**, 135–224.
 10. Jayswal, A. and Chudasama, U. (2007) Sorption of water soluble dyes using zirconium-hydroxy ethylidene diphosphonate from aqueous solution. *Malaysian Journal of Chemistry*, **9**(1), 1–9.
 11. Mumin, A., Akhter, K. F., Abedin, Z. and Hossain, Z. (2006) Determination and characterization of caffeine in tea, coffee and soft drinks by solid phase extraction and high performance liquid chromatography (SPE–HPLC). *Malaysian Journal of Chemistry*, **8**(1), 045–051.
 12. Singh, N. B., Nagpal, G., Agrawal, S. and Rachna (2018) Water purification by using Adsorbents. *Environmental Technology and Innovation*, **11**, 187–240.
 13. Husien, S., El-taweel, R. M., Salim, A. I., Fahim, I. S., Said, L. A. and Radwan, A. G. (2022) Review of activated carbon adsorbent material for textile dyes removal: Preparation, and modelling. *Current Research in Green and Sustainable Chemistry*, **5**, 100325.
 14. Rao, P. R., Eranna, B. C., Berekute, A. K. and Duraisamy, R. (2018) Studies on separation of heavy metals from aqueous solutions using biosorbents. *Malaysian Journal of Chemistry*, **20**(1), 128–137.
 15. Rashid, S., Mazlan, N. A., Sapari, J. M., Raoov Ramachandran, M. and Pandian Sambasevam, K. (2018) Fabrication of magnetic nanoparticles coated with polyaniline for removal of 2, 4-dinitrophenol. *Journal of Physics: Conference Series*, **1123**, 012015.
 16. Madan, S., Shaw, R., Tiwari, S. and Tiwari, S. K. (2019) Adsorption dynamics of Congo red dye removal using ZnO functionalized high silica zeolitic particles. *Applied Surface Science*, **487**, 907–917.
 17. Ewis, D., Ba-Abbad, M. M., Benamor, A. and El-Naas, M. H. (2022) Adsorption of organic water pollutants by clays and clay minerals composites: A comprehensive review. *Applied Clay Science*, **229**, 106686.
 18. Awad, A. M., Shaikh, S. M., Jalab, R., Gulied, M. H., Nasser, M. S., Benamor, A. and Adham, S. (2019) Adsorption of organic pollutants by natural and modified clays: a comprehensive review. *Separation and Purification Technology*, **228**, 115719.
 19. Najafi, H., Farajfaed, S., Zolgharnian, S., Mosavi Mirak, S. H., Asasian-Kolur, N. and Sharifian, S. (2021) A comprehensive study on modified-pillared clays as an adsorbent in wastewater treatment processes. *Process Safety and Environmental Protection*, **147**, 8–36.
 20. Gómez-Pastora, J., Bringas, E. and Ortiz, I. (2014) Recent progress and future challenges on the use of high performance magnetic nano-adsorbents in environmental applications. *Chemical Engineering Journal*, **256**, 187–204.
 21. Mohamad, S., Abu Bakar, N. K., Ishak, A. R., Surikumaran, H., Pandian, K., Raoov, M. and Chandrasekaram, K. (2014) Removal of Phosphate by Paper Mill Sludge: Adsorption Isotherm and Kinetic Study. *Asian Journal of Chemistry*, **26**(12), 3545–3552.

- 156 Imane Lacene Necer, Khalil Oukebdane and Mohamed Amine Didi
- Enhanced Removal of Bemacid Blue Anthraquinone Dye by Magnetic Nanocomposite Bentonite-Fe₃O₄: Equilibrium, Kinetic and Thermodynamic Studies
22. Oukebdane, K., Lacene Necer, I. and Didi, M. A. (2022) Binary comparative study adsorption of anionic and cationic Azo-dyes on Fe₃O₄-Bentonite magnetic nanocomposite: Kinetics, Equilibrium, Mechanism and Thermodynamic study. *Silicon*, 1–14.
 23. Djebbar, M., Djafri, F., Bouchekara, M. and Djafri, A. (2012) Adsorption of phenol on natural clay. *Applied Water Science*, **2**(2), 77–86.
 24. Massart, R. (1981) Preparation of aqueous magnetic liquids in alkaline and acidic media. *IEEE Transactions on Magnetics*, **17**, 1247–1248.
 25. Daoush, W. M. (2017) Co-precipitation and magnetic properties of magnetite nanoparticles for potential biomedical applications. *Journal of nanomedicine research*, **5**, 00118.
 26. Achour, S., Amokrane, S., Chegrouche, S., Nibou, D. and Baaloudj, O. (2021) Artificial neural network modeling of the hexavalent uranium sorption onto chemically activated bentonite. *Research on Chemical Intermediates*, **47**, 4837–4854.
 27. Şans, B. E., Esenli, F., Kadir, S. and Elliott, W. C. (2015) Genesis of smectite in siliciclastics and pyroclastics of the Eocene İslambeyli Formation in the Lalapaşa region, NW Thrace, Turkey. *Clay Minerals*, **50**, 459–483.
 28. Grim, R. and Guven, N. (1978) Bentonite: Geology, Clay Mineralogy Properties and Users. *Elsevier Science Publishing*, 256.
 29. Decarreau, A., Grauby, O. and Petit, S. (1992) The actual distribution of octahedral cations in 2:1 clay minerals. Results from clay synthesis. *Applied Clay Science*, **7**, 147–167.
 30. Alekseeva, O. V., Noskov, A. V. and Agafonov, A. V. (2022) Structure, physicochemical properties, and adsorption performance of the ethyl cellulose/bentonite composite films. *Cellulose*, **29**, 3947–3961.
 31. Qiao, Z., Liu, Z., Zhang, S., Yang, Y., Wu, Y., Liu, L. and Liu, Q. (2020) Purification of montmorillonite and the influence of the purification method on textural properties. *Applied clay science*, **187**, 105491.
 32. Belachew, N. and Bekele, G. (2020) Synergy of magnetite intercalated bentonite for enhanced adsorption of congo red dye. *Silicon*, **12**, 603–612.
 33. Lou, Z., Zhou, Z., Zhang, W., Zhang, X., Hu, X., Liu, P. and Zhang, H. (2015) Magnetized bentonite by Fe₃O₄ nanoparticles treated as adsorbent for methylene blue removal from aqueous solution: Synthesis, characterization, mechanism, kinetics and regeneration. *Journal of the Taiwan Institute of Chemical Engineers*, **49**, 199–205.
 34. Wei, Y., Han, B., Hu, X., Lin, Y., Wang, X. and Deng, X. (2012) Synthesis of Fe₃O₄ nanoparticles and their magnetic properties. *Procedia engineering*, **27**, 632–637.
 35. Devi, S. M., Nivetha, A. and Prabha, I. (2019) Superparamagnetic properties and significant applications of iron oxide nanoparticles for astonishing efficacy-a review. *Journal of Superconductivity and Novel Magnetism*, **32**, 127–144.
 36. Wang, W., Feng, Q., Dong, F., Li, H. and Zhao, X. (2010) Preparation and properties of magnetic bentonite. *Journal of the Chinese Ceramic Society*, **38**(4), 684–688.
 37. Masanizan, A., Lim, C. M., Kooh, M. R. R., Mahadi, A. H. and Thotagamuge, R. (2021) The Removal of Ruthenium-Based Complexes N3 Dye from DSSC Wastewater Using Copper Impregnated KOH-Activated Bamboo Charcoal. *Water, Air, & Soil Pollution*, **232**(9), 1–15.
 38. Bakatula, E. N., Richard, D., Neculita, C. M. and Zagury, G. J. (2018) Determination of point of zero charge of natural organic materials. *Environmental Science and Pollution Research*, **25**, 7823–7833.
 39. Errais, E., Duplay, J., Darragi, F., M'Rabet, I., Aubert, A., Huber, F. and Morvan, G. (2011) Efficient anionic dye adsorption on natural untreated clay: Kinetic study and thermodynamic parameters. *Desalination*, **275**, 74–81.
 40. Chinoune, K., Bentaleb, K., Bouberka, Z., Nadim, A. and Maschke, U. (2016) Adsorption of reactive dyes from aqueous solution by dirty bentonite. *Applied clay science*, **123**, 64–75.
 41. Liu, Q., Yang, B., Zhang, L. and Huang, R. (2015) Adsorption of an anionic azo dye by cross-linked chitosan/bentonite composite. *International journal of biological macromolecules*, **72**, 1129–1135.
 42. Adeyemo, A. A., Adeoye, I. O. and Bello, O. S. (2017) Adsorption of dyes using different types of clay: a review. *Applied water science*, **7**, 543–568.
 43. Garg, V., Kumar, R. and Gupta, R. (2004) Removal of malachite green dye from aqueous solution by adsorption using agro-industry waste: a case study of Prosopis cineraria. *Dyes and Pigments*, **62**(1), 1–10.
 44. Guechi, E. K. and Hamdaoui, O. (2016) Sorption of malachite green from aqueous solution by potato peel: kinetics and equilibrium modeling using non-linear analysis method. *Arabian Journal of Chemistry*, **9**, 416–424.

45. Hashem, F. S. and Amin, M. S. (2016) Adsorption of methylene blue by activated carbon derived from various fruit peels. *Desalination and Water Treatment*, **57**, 22573–22584.
46. Singh, T. S. and Pant, K. K. (2006) Kinetics and Mass Transfer Studies on the Adsorption of Arsenic onto Activated Alumina and Iron Oxide Impregnated Activated Alumina. *Water Quality Research Journal*, **41**, 147–156.
47. Sharma, A., Mangla, D., Choudhry, A., Sajid, M. and Chaudhry, S. A. (2022) Facile synthesis, physico-chemical studies of Ocimum sanctum magnetic nanocomposite and its adsorptive application against Methylene blue. *Journal of Molecular Liquids*, **362**, 119752.
48. Seliman, A. F., Lasheen, Y. F., Youssief, M. A. E., Abo-Aly, M. M. and Shehata, F. A. (2014) Removal of some radionuclides from contaminated solution using natural clay: bentonite. *Journal of Radioanalytical and Nuclear Chemistry*, **300**, 969–979.
49. Hamzenejad Taghlidabad, R., Sepehr, E., Khodaverdiloo, H., Samadi, A. and Rasouli-Sadaghiani, M. H. (2020) Characterization of cadmium adsorption on two cost-effective biochars for water treatment. *Arabian journal of geosciences*, **13**, 448.
50. Gheju, M., Balcu, I. and Mosoarca, G. (2016) Removal of Cr (VI) from aqueous solutions by adsorption on MnO₂. *Journal of hazardous materials*, **310**, 270–277.
51. Snik, A., Jioui, I., Larzek, M., Assabbane, A. and Zahouily, M. (2022) Cationic Dye Removal (Methylene Blue) from Aqueous Solution Using the Ecologically Friendly Alginate/Hydroxyapatite/Graphene Oxide Nanocomposite Hydrogel Beads. *Water, Air, & Soil Pollution*, **233**, 1–30.
52. Gayathri, K. and Palanisamy, N. (2019) Methylene blue adsorption onto an eco-friendly modified polyacrylamide/graphite composites: Investigation of kinetics, equilibrium, and thermodynamic studies. *Separation Science and Technology*, **55**, 266–277.